



In-situ grown MgO-ZnO ceramic coating with high thermal emittance on Mg alloy by plasma electrolytic oxidation



Hang Li^a, Songtao Lu^{a,*}, Wei Qin^b, Xiaohong Wu^{a,*}

^a School of Chemistry and Chemical Engineering, Harbin Institute of Technology, Harbin, Heilongjiang 150001, PR China

^b School of Materials Science and Engineering, Harbin Institute of Technology, Harbin, Heilongjiang 150001, PR China

ARTICLE INFO

Keywords:

Mg alloy
Plasma electrolytic oxidation
ZnO
Emittance
Solar absorptance

ABSTRACT

Intense solar radiation and internal heat generation determine the equilibrium temperature of an in-orbit spacecraft. Thermal control coatings with low solar absorptance and high thermal emittance effectively maintain the thermal equilibrium within safe operating limits for exposed, miniaturized and highly integrated components. A novel ceramic coating with high thermal emittance and good adhesion was directly prepared on the Mg substrate using an economical process of controlled plasma electrolytic oxidation (PEO) in the electrolyte containing ZnSO₄. XRD and XPS results showed that this coating was mainly composed of the MgO phase as well as an unusual ZnO crystalline phase. The adhesive strength between the coating and substrate determined by a pull-off test revealed an excellent adhesion. Thermal and optical properties test revealed that the coating exhibited a high infrared emittance of 0.88 (2–16 μm) and low solar absorptance of 0.35 (200–2500 nm). The result indicated that the formation of ZnO during the PEO process played an important role in the improvement of the coating emittance. The process developed provides a simple surface method for improving the thermal emittance of Mg alloy, which presents a promising application prospect in the thermal management of the spacecraft.

1. Introduction

Orbital spacecraft suffers the extreme temperature cycling owing to direct sun load on one side and deep cold space on the other, which reduces the component lifetime [1,2]. As a result, effective thermal prevention measures are very necessary to ensure the normal operation of devices and instruments in the spacecraft [3]. A common passive method is the thermal control coating, which provides the radiative pathway to dissipate heat without energy consumption [4]. Mostly, exposure components in the spacecraft are made of Al alloy, which normally employed the white coating with a low solar absorptance (α_s) and a high infrared emittance (ϵ) for a purpose of thermal control [5]. Currently, white anodizing and ZnO white paints are widely used in spacecraft. C.S. Kumar et al. fabricated white anodizing coatings on Al alloy with a α_s -value of 0.16 and a ϵ -value of 0.80 [6]. Yet white paints in hash space environment easily run into the thermal-optical degradation, namely α_s -value increasing and ϵ -value decreasing, which would directly reduce the spacecraft lifetime [7,8].

With the rapid development of science and technology, light-weight materials are in great demand for the spacecraft application for the purpose of increasing the payload ratio and reducing energy consump-

tion. Mg alloy has been considered as a promising material for the spacecraft owing to its low density, high specific strength and excellent electromagnetic shielding [9–11]. For example, an electronic equipment cabinet used in Chang'3 Rover was fabricated by Mg alloy [12]. Recently, more certain components in this type light-weight engine are made of Mg alloy rather than Al alloy, e.g. the engine block, oil pan and front engine cover [13,14]. However, an important disadvantage of Mg alloy is the high chemical activity which seriously hinders its future application [15]. Thermal control coatings prepared on Mg alloy using the anodizing and painting are easily led to the property degradation in the space environment and show relatively weak adhesion with the substrate [16,17]. Therefore, it is of great significance to develop a novel technique for thermal control coating to increase the adhesive strength.

The PEO technique enables to in-situ generate the ceramic coating with designed chemical compositions on Mg, Ti and Al valve metals [18]. The prepared coatings exhibit good insulation, biocompatibility, wear resistance and excellent adhesion strength with the substrate [11,19]. This method is an advanced high voltage anodizing process in which the generation of micro discharges on the anodic electrode is attributed to the existence of ceramic coating dielectric breakdown

* Corresponding authors.

E-mail addresses: lusongtao@hit.edu.cn (S. Lu), wuxiaohong@hit.edu.cn (X. Wu).

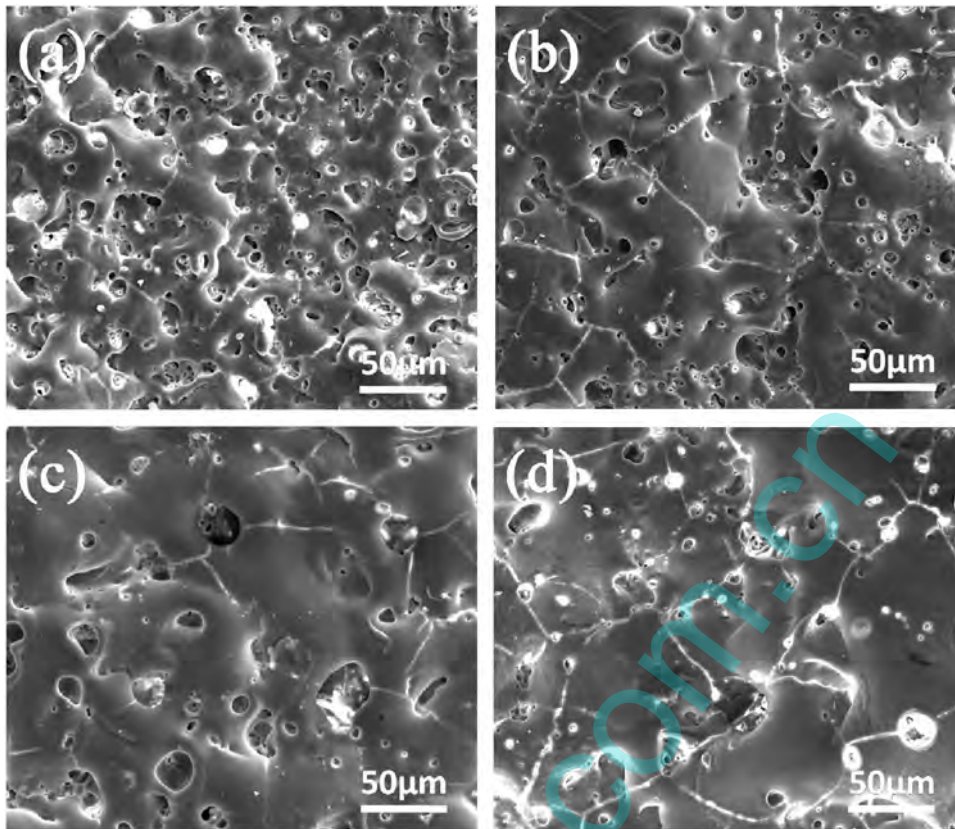


Fig. 1. Surface SEM images of PEO coatings prepared under different concentrations of ZnSO_4 : (a) 0 g/L; (b) 2 g/L; (c) 4 g/L; (d) 6 g/L.

[20]. The electrolyte for PEO is usually the non-hazardous alkaline-based system, consisting of silicate, phosphate, hydroxide, fluoride and/or organic additives [21]. The environmentally friendly process can reduce the costs and fulfill the required performance in one step [22]. Moreover, the PEO approach significantly minimizes the risk of the premature fatigue failure for the substrate material [23]. The report showed that the bonding strength between the PEO coating and the Mg substrate was strong [24]. J. Chen et al. prepared thermal control coatings with good adhesion on AZ91 Mg alloy via the PEO method, yet ϵ -values were relatively low [25]. In the PEO process, the elements in the substrate and the electrolyte were incorporated into the coating via the plasma electro-chemical reaction [19,25]. Thus, the excellent thermal control coating on Mg alloy can be fabricated by changing the electrolyte composition. In this paper, a novel ZnO-containing thermal control ceramic coating with high thermal emittance and good adhesion on AZ31 Mg alloy was prepared by the PEO technique in the electrolyte containing Zn^{2+} ions. The effect of Zn^{2+} ions on the structure, composition, adhesive strength and thermal control performance of the PEO coating has been studied.

2. Experiment details

2.1. Preparation procedure of PEO coatings

Plate samples of AZ31 Mg alloy (wt%: 0.35Mn, 0.4Zn, 3.5Al, Mg balance) with a dimension of 4 cm×4 cm×0.2 cm were used as the substrate material. Prior to the PEO treatment, metal samples were polished using 2000 mesh SiC papers, and ultrasonically degreased in acetone and then cleaned with the distilled water. The 10 kW bipolar pulsed power supply was employed to carry out the PEO reaction of the samples in the electro bath of the stainless steel serving as the cathode. The cooling water flow was used to maintain the reaction temperature below 30 °C. The plasma electrolysis mechanism of the PEO process

was detailed described by the Matthews's group [26]. The power parameters were fixed at the pulse frequency of 50 Hz, the current density of 15 A/dm², and the duty ratio of 45%. The duration time of the oxidation process was 10 min. The electrolyte solutions contained 30 g/L $\text{Na}_5\text{P}_3\text{O}_{10}$ and 5 g/L NaOH, mixed with various concentrations of ZnSO_4 (0, 2, 4 and 6 g/L). After the PEO process, the obtained samples were rinsed with water and then dried in the air.

2.2. Microstructure and composition characterizations

The coating microstructure was observed by SEM (Hitachi, S-570). 3D surface structure and Root-Mean-Square (rms) roughness was measured by AFM (CSPM 5500, Beig). The crystal structure of the obtained coating was characterized by XRD (Rigaku, Dmax-3B), with a Cu K α radiation ($\lambda=1.54060 \text{ \AA}$). The chemical composition and valence state were investigated by XPS (America, PHI5700) with an Al K α X-ray source ($h\nu=1486 \text{ eV}$). According to ISO 14916, the adhesive strength of four samples, prepared under four various concentrations of ZnSO_4 , were tested by a direct pull-off approach [27]. The pull-off tests of all samples were performed at the rate of 0.2 mm/min using the WDW-100 universal testing machine. The spectral emittance values at 2–16 μm were examined by an infrared reflectometer (Gier-Dunkle DB-100) and the α_s -values in the 200–2500 nm wavelength range by a UV–VIS–NIR spectrophotometer (Perkin Elmer Lambda 950) with an integrating sphere. The total α_s -value can be calculated by the following formula [25]:

$$\alpha_s = 1 - \rho_s = 1 - \frac{\int_{\lambda_1}^{\lambda_2} \rho_\lambda S_\lambda d\lambda}{\int_{\lambda_1}^{\lambda_2} \rho_\lambda d\lambda} \quad (1)$$

Here, ρ_s is the reflectance of the coating; S_λ is the spectrum of the solar radiation; ρ_λ is the spectral reflectance in the 200–2500 nm range.

3. Results and discussion

3.1. Surface microstructure and voltage-time response

Fig. 1 shows the superficial microstructure of the ceramic coatings prepared under various concentrations of ZnSO_4 . As can be seen from Fig. 1, the as-prepared coatings show a typical porous structure characteristic of the PEO coating. Many micro-porous with different shapes and sizes distributed randomly, which corresponded with the plasma discharge channels on the anode during the PEO process. Some cracks were attributed to the existence of the thermal stress induced by the rapid solidification [28]. With the increase of ZnSO_4 concentration, the number of pores on the surface becomes less due to the enhancement of the PEO reaction reflected by the high anode voltage. An important characteristic of the PEO process is the spark phenomenon during the discharge process. The optical and acoustic features of the spark are directly related to the anode voltage [29]. High anode voltage indicates that there is the high energy on the surface of the anode, which initiates the more violent discharges to enhance the electrochemical oxidation. As a result, the micro-plasma discharge process was enhanced and consequently more molten oxides were ejected from the discharge channels to seal part of the micro-pores.

This also can be confirmed by the dependency of anode voltage on the processing time obtained during the PEO process, and the results are shown in Fig. 2. The voltage ascended linearly similar to the conventional anodizing at the initial 30 s and then decreased slowly due to a stable growth rate of the coating. Additionally, it can be noted that the voltage increased with the addition of Zn^{2+} ions indicating that the coating growth rate after doping was raised. Zn^{2+} ions in the electrolyte reacted with OH^- ions to generate $[\text{Zn}(\text{OH})_4]^{2-}$ anions, which were adsorbed on the anodic surface to increase the electrical resistance of the anode. Thus, higher energy input was needed for the dielectric breakdown, which directly caused more violent micro-discharges and the higher anode voltage than that without Zn^{2+} ions. More energy input promoted the conversion of the substrate surface into more melted magnesium oxides, which rapidly solidified under the cold quenching effect of the adjacent electrolyte to raise the growth rate of the coating [30]. Moreover, $[\text{Zn}(\text{OH})_4]^{2-}$ anions were oxidized to form ZnO, contributing to the increase of the coating thickness.

Therefore, the voltage-time behavior for this PEO process was dependent on the concentration of $[\text{Zn}(\text{OH})_4]^{2-}$ anions in the electrolyte. It was observed from Fig. 2 that the voltage-time curve at 4 g/l ZnSO_4 has little difference with that at 6 g/L, indicating that $[\text{Zn}(\text{OH})_4]^{2-}$ concentration may reach the saturation at 4 g/L in the electrolyte. With the concentration of ZnSO_4 up to 6 g/L, Zn^{2+} ions can combine with OH^- ions to generate the sediment $\text{Zn}(\text{OH})_2$ [31].

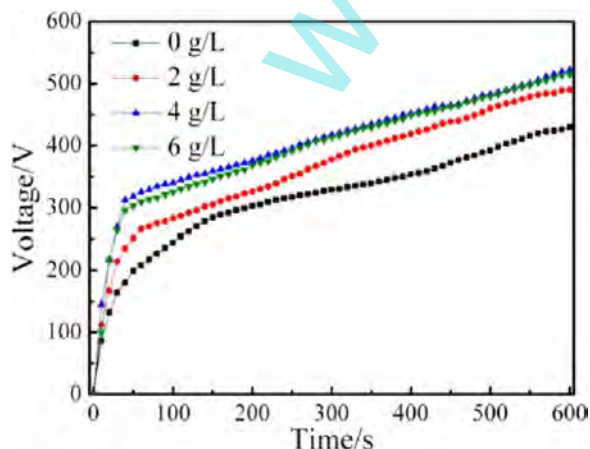


Fig. 2. Voltage-time curves during the PEO process under different concentrations of ZnSO_4 .

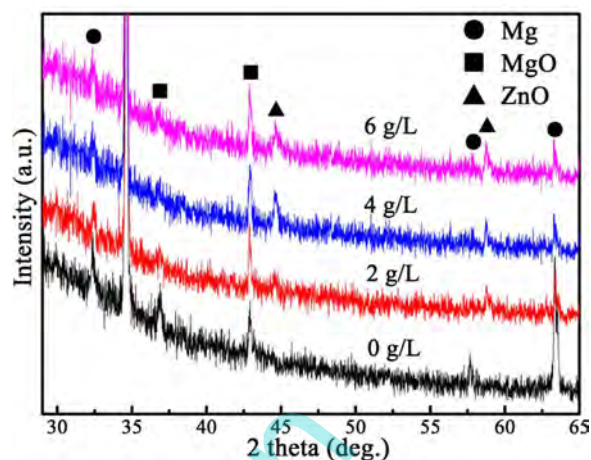


Fig. 3. XRD patterns of PEO coatings obtained under different ZnSO_4 addition.

However, the difference on the microstructure of the coatings prepared at 4 g/L and 6 g/L ZnSO_4 can be ascribed to the change of the electrolyte pH. The generation of $\text{Zn}(\text{OH})_2$ decreased OH^- concentration to lead to the acidification of the electrolyte [32]. Accordingly, the concentration of H^+ ions from the hydrolysis can rise, which caused the erosion of the coating surface as well as the increase of the roughness.

3.2. Phase and chemical composition

Fig. 3 shows the XRD spectrum of the ceramic coatings obtained at different ZnSO_4 concentrations. It revealed that the PEO coating was mainly composed of Mg and the periclase MgO phase, as well as the ZnO crystalline phase. The substrate peaks were reflected in the patterns due to the porous structure and weak zones of the coating easily leading to X-ray to reach the internal substrate [33]. These crystal planes of MgO peaks corresponding to (111) and (200) are well matched with the standard JCPDS No. 45–0946. Interestingly, the diffraction peaks locating at 44.6° and 58.8° are consistent with an unusual ZnO phase matched with JCPDS No. 21–1486. This crystalline structure also was detected by some researchers [34,35]. It has been reported that no information in the JCPDS file is provided about the crystal plane.

To further investigation the chemical composition of the coating, XPS analysis was used to characterize the element and composition. Fig. 4a depicts the survey spectrum of the coating prepared at 4 g/L ZnSO_4 , in which Mg, Na, O, P, C and Zn elements were detected. The adventitious carbon C1s peak at 284.6 eV was referred to calibrate all the binding energies. The presence of Mg originated from the substrate and others from the electrolyte. The peak of Zn2p was splitted into the 2p_{1/2} and 2p_{3/2} core levels respectively located at 1044.4 eV and 1021.5 eV with a spin orbit splitting of 22.9 eV, confirming the presence of ZnO [36]. For the metal oxides, the electro-negativity of lattice metal ions directly influences the valence electron density of the adjacent oxide ions [37]. As the reduction of the electro-negativity for the metal ions, the electron density of the adjacent lattice oxide ions would increase. The difference of the binding energy for this MgO–ZnO ceramic coating is about 0.4 eV lower than that of pure ZnO [38], which indicates that the valence electron density of Zn ions increases. It is well-known that the electro-negativity of Mg is 1.31 lower than that of Zn (1.65). It may be deduced that the partial Zn ions entered into the matrix of the MgO lattice during the PEO process, due to the higher valence electron density of Zn in the Zn–O–Mg bond compared with that of the Zn–O–Zn bond in pure ZnO.

O1s peaks can be deconvoluted into two components. The peak A located at 531.2 eV corresponded to O^{2-} in MgO, and the peak B at 532.9 eV is related to Zn–O bonding attributed to the formation of ZnO [39,40]. Yet according to the literature, the binding energies of the O1s

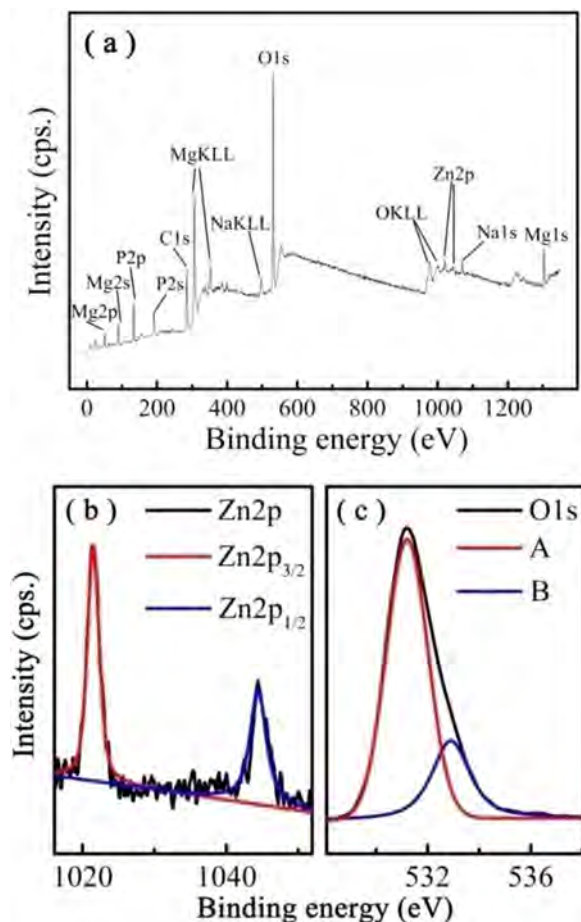
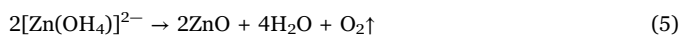


Fig. 4. XPS spectra of the PEO coating fabricated at 4 g/L ZnSO₄: (a) survey scan, (b) Zn2p and (c) O1s.

peaks belonging to MgO and ZnO are 529.2 eV and 530.2 eV, respectively [41,42]. In comparison with the O1s peaks in Fig. 4c, two peaks with higher binding energies may be associated with the dissociated or adsorbed oxygen species on the surface of the coating, e.g., adsorbed H₂O or O₂ [43].

Similar to the electrochemical mechanism of the classical anodizing, the groups and ions with the negative charge under the electric field action move toward the anode surface and participate in the PEO reaction. Zn²⁺ ions in the electrolyte reacted with OH⁻ to form [Zn(OH)₄]²⁻, which would migrate to the anodic surface under the action of the intense electric field. And then [Zn(OH)₄]²⁻ anions on the coating/ electrolyte interface were oxidized to generate ZnO at high temperature and pressure. In the PEO reaction, the electrochemical reactions are given below:



3.3. Adhesive strength of the PEO coatings

One important mechanical property of thermal control coatings is the adhesive strength between the coating and substrate, which should be taken into account in the practical application. According to ISO 14916, test results of the adhesive strength for all samples are shown in

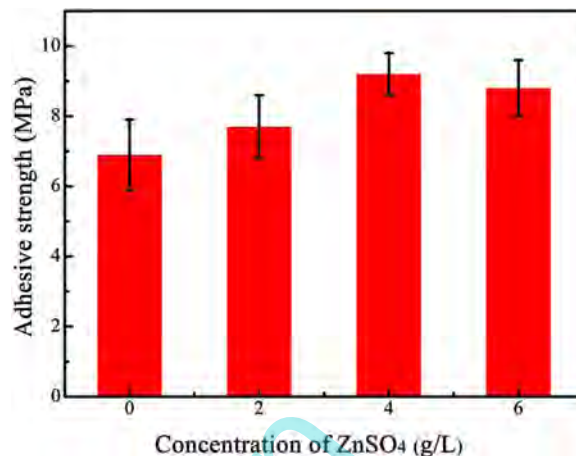


Fig. 5. Adhesion strength of the coatings obtained at different ZnSO₄ addition.

Fig. 5. Increasing the concentration of ZnSO₄, the adhesive strength is 6.9, 7.7, 9.2 and 8.8 MPa, respectively. All the ceramic coatings show satisfactory adhesive strength in comparison to anodized and painting coatings. It can be attributed to the “quenching effect” during the PEO process. The plasma discharge can lead to an extreme high temperature and pressure on the anode surface, while the electrolyte is cooling. This high temperature difference makes the molten surface strongly adhere to the Mg alloy substrate [44,45].

The mechanical mechanism of adhesion between the coating and substrate is associated with the surface roughness and the compactness of the coating [46,47]. The intrinsically high surface energy of atoms on a rough surface can facilitate the enhancement of the adhesive strength at the coating-binder interface. Moreover, high compactness of the coating can increase the cohesive strength, which leads to the increase of adhesion at the internal structure of the coating and the metal-coating interface. As a consequence, high surface roughness and compactness of the coating are able to enhance the adhesive strength. With the concentration of ZnSO₄ up to 4 g/L, the roughness and compactness of the coating gradually increased, as shown in Fig. 7. Thus, the adhesive strength was enhanced due to high specific surface area and cohesive strength. However, as the concentration continued to increase, the compactness of the coating presented a decrease which was the main factor of the slight reduction for the adhesive strength of the coating obtained at 6 g/L ZnSO₄.

3.4. thermal and optical performances

The spectral emittance values for the PEO coatings and the bare substrate at the wavelength of 2–16 μm are represented in Fig. 6. Clearly the emittance of Mg alloy was greatly improved after the PEO oxidation. With increasing the concentration of ZnSO₄, the average emittance values of the PEO coatings were 0.68, 0.79, 0.88 and 0.88, respectively. Compared with the coating without ZnO, the emittance was gradually increased with the adding of Zn²⁺ ions. According to the infrared radiation theory, the emittance of the coating is mostly influenced by their thickness, surface structure and composition [48–50].

In order to investigate the influence of ZnSO₄ on the emittance, the thickness and surface roughness of the coating were measured firstly. The variation of the thickness can be observed from the cross-section SEM images and the surface structure was tested by a scanning probe microscope system, as shown in Fig. 7. The coating thickness increased with increasing the ZnSO₄ concentration and was all the more than 30 μm. And a thicker coating could effectively prevent the transmission of the light wave [51]. The relationship between the emittance and thickness was described using the following equation [52]:

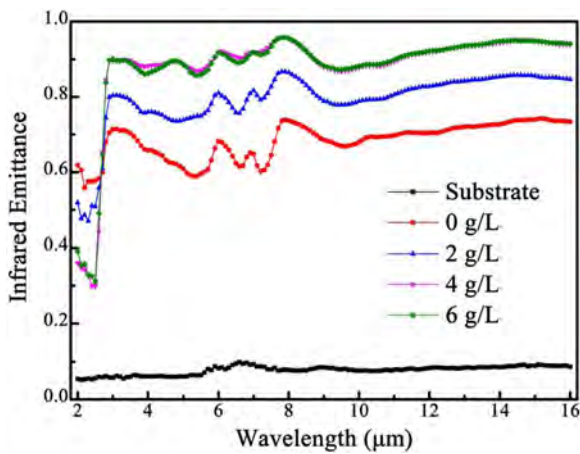


Fig. 6. Spectral emittance values of the substrate and PEO coatings prepared under different concentrations of ZnSO₄.

$$\epsilon = \frac{(1-\rho_c)(e^{A\beta d} - \rho_s)}{e^{A\beta d} - \rho_c\rho_s} = (1 - \rho_c) \left[1 - \frac{\rho_s(1-\rho_c)}{e^{A\beta d} - \rho_c\rho_s} \right] \quad (6)$$

where, ρ_c is the coating reflectance; ρ_s is the substrate reflectance; d is the coating thickness; and β is the Beer-Lambert absorption coefficient. Thus, the emittance increases with the increase of the thickness, which is consistent with our experimental results. Fig. 7b shows the AFM images of the coatings fabricated under different ZnSO₄ concentration. It can be observed that all the coatings displayed a rough surface with many peaks and valleys. As the adding of Zn²⁺ ions, the rms roughness of the coatings was 32.8, 34.6, 37.7 and 38.3 nm, respectively. The rough surface structure can directly increase the specific surface area of the coating, which can cause more heat radiated from the surface. The correlation between the thermal emittance and roughness is expressed below [53]:

$$\epsilon = 1 - \rho_p = 1 - \rho_R \exp\left(-\frac{4\pi R}{\lambda}\right)^2 \quad (7)$$

In this equation, ρ_p and ρ_R are the reflectance of a polished and rough surface, respectively; R is the roughness and λ is the wavelength. According to Eq. (7), high roughness leads to high emittance. Therefore, the enhancement of the thermal emittance can be attributed to the increase of the thickness and roughness which was induced from the existence of Zn²⁺ ions in the electrolyte. Furthermore, ZnO usually served as a white pigment in thermal control coatings due to its non-toxic and wider forbidden band [54,55]. Besides, ZnO itself possesses a

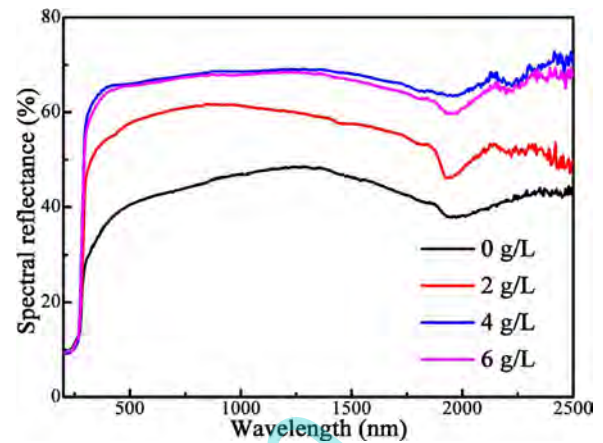


Fig. 8. Diffuse reflectance spectrum of the PEO coating prepared under different ZnSO₄ concentrations.

high emissivity value [56], which can contribute to enhance the coating emittance. Meanwhile, Fig. 8 showed the diffuse reflectance spectrum of the coating prepared at different concentration of ZnSO₄. According to Eq. (1), the calculated α_s -values with the increase of ZnSO₄ concentration are 0.58, 0.46, 0.35 and 0.36, respectively. Compared with other coatings in references [6,25,57–61] showed in Table 1, the coating prepared by our own method presents better thermal control performance. The solar absorptance of the coatings obtained with Zn²⁺ ions was lower than that without Zn²⁺ ions due to the high refractive index of ZnO [62]. However, the difference of the absorptance between the coatings obtained at 4g/L and 6g/L ZnSO₄ was mainly attributed to the different roughness. High surface roughness can reduce the reflectance of the coating. The PEO coating fabricated at 4g/L ZnSO₄ demonstrated the lowest solar absorptance of 0.35, which accorded with the requirement of thermal control coatings on the spacecraft [63]. Especially, this ceramic coating with excellent adhesion and low absorptance-emittance ratio can play an important role in the improvement of the thermal control design on the spacecraft.

4. Conclusions

In summary, a thermal control ceramic coating with high thermal emittance and good adhesion was in-situ fabricated by a rapid and simply PEO technique in the electrolyte containing Na₅P₃O₁₀, NaOH and ZnSO₄. XRD and XPS results revealed that the PEO coating was mainly composed of ZnO and MgO. A pull-off test showed that all coatings possess an

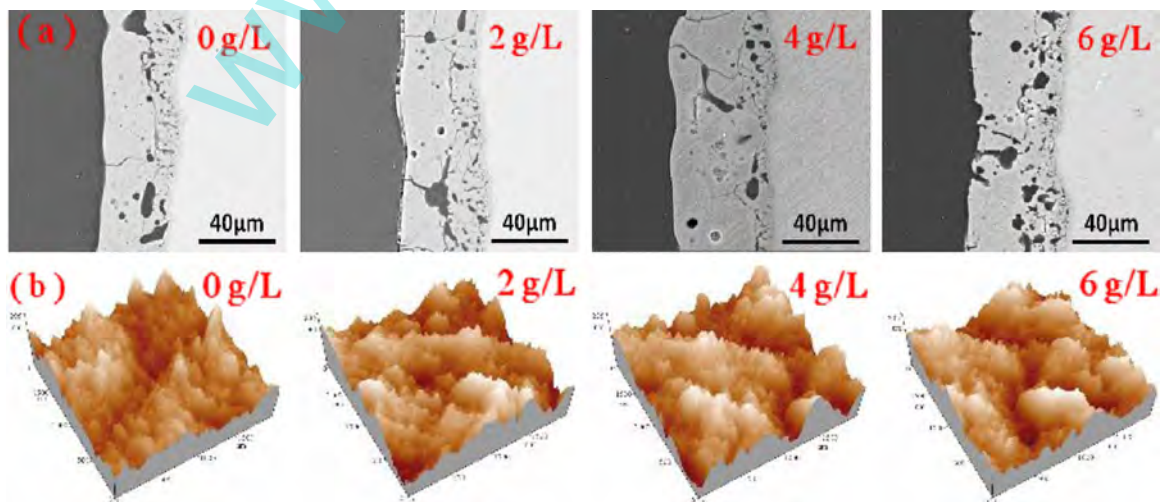


Fig. 7. Cross-section and AFM surface images of PEO coatings obtained in the electrolytes with different ZnSO₄ concentrations.

Table 1
Comparison of α_s and ε of the coatings prepared on Al and Mg alloys.

Alloy	Technique	α_s	ε	Refs.
2024 Al	Anodizing	0.16	0.80	[6]
6061 Al	PEO	—	0.76 (4–16 μm)	[57]
2024 Al	PEO	—	0.85 (8–20 μm)	[58]
6061 Al	Gravity pre-deposition + PEO	≥ 0.85	≥ 0.90	[59]
AZ31 Mg	PEO	0.94	0.83	[60]
AZ91D Mg	PEO	—	0.80 (8–20 μm)	[61]
AZ91D Mg	PEO	0.439	0.80	[25]

excellent adhesive strength. After the incorporation of ZnO in the PEO coating, the infrared emittance improved from 0.68 to 0.88. The thickness and roughness of the coating were mostly influenced by the concentration of Zn^{2+} ions. When the concentration of Zn^{2+} ions was 4 g/L, the PEO coating showed the strongest adhesive strength of 9.2 MPa, and its infrared emittance and solar absorptance reached 0.88 and 0.35, respectively. The results indicated that the ceramic coating can be used as the promising thermal control coating. It is believed that this technique may open a new approach to expand the application of Mg alloy.

Acknowledgement

This work was supported by the Fundamental Research Funds for the Central Universities (No. HIT.BRETHIII.201224 and 201312), Program for Innovation Research of Science in Harbin Institute of Technique (PIRS of HIT-No. 201506) and Excellent Youth Foundation of Heilongjiang Scientific Committee (No. JC2015010).

References

- [1] H. Xing, H. Zhao, Y. Zhang, Q. Zhang, *Acta Astronaut.* 71 (2012) 99–108.
- [2] V. Heydari, Z. Bahreini, M. Heidari, A. Sedrpoushan, *J. Coat. Technol. Res.* 13 (2016) 727–733.
- [3] S. Wijewardane, D.Y. Goswami, *Renew. Sust. Energy Rev.* 16 (2012) 1863–1873.
- [4] N. Kiamarsipour, R.S. Razavi, K. Ghani, *Dyes Pigment.* 96 (2013) 403–406.
- [5] K.A.J. Doherty, J.G. Carton, A. Norman, T. McCaul, B. Twomey, K.T. Stanton, *Acta Astronaut.* 117 (2015) 430–439.
- [6] C.S. Kumar, A.K. Sharma, K.N. Mahendra, S.M. Mayanna, *Sol. Energ. Mat. Sol. C* 60 (2000) 51–57.
- [7] H.W. Babel, C. Jones, K. David, *Acta Astronaut.* 39 (1996) 369–379.
- [8] G. Bitettia, M. Marchettia, S. Miletia, F. Valentea, S. Scaglione, *Acta Astronaut.* 60 (2007) 166–174.
- [9] M. Mondet, E. Barraud, S. Lemonnier, J. Guyon, N. Allain, T. Grosdidier, *Acta Mater.* 119 (2016) 55–67.
- [10] S.H. Abdollahi, F. Karimzadeh, M.H. Enayati, *J. Alloy. Compd.* 623 (2015) 335–341.
- [11] H. Li, S. Lu, W. Qin, L. Han, X. Wu, *Acta Astronaut.* 116 (2015) 126–131.
- [12] C. Pan, Q. Liu, X. Zhang, Q. He, Y. Wu, *Chin. Astron. Astrophys.* 40 (2016) 236–246.
- [13] A.A. Luo, *J. Magn. Alloy.* 1 (2013) 2–22.
- [14] R. Dhingra, S. Das, *J. Clean. Prod.* 85 (2014) 347–358.
- [15] L. Niu, S.H. Chang, Y. Su, D. Han, G. Li, *J. Alloy. Compd.* 635 (2015) 11–15.
- [16] J.M. Wheeler, J.A. Curran, S. Shrestha, *Surf. Coat. Technol.* 207 (2012) 480–488.
- [17] N.V. Phuong, S. Moon, *Prog. Org. Coat.* 89 (2015) 91–99.
- [18] H.N. Vatan, R. Ebrahimi-kahrizangi, M. Kasiri-asgarani, *J. Alloy. Compd.* 683 (2016) 241–255.
- [19] S. Liu, B. Li, C. Liang, H. Wang, Z. Qiao, *Appl. Surf. Sci.* 362 (2016) 109–114.
- [20] D. Veys-Renaux, E. Rocca, G. Henrion, *Electrochem. Commun.* 31 (2013) 42–45.
- [21] C. Blawert, W. Dietzel, E. Ghali, G. Song, *Adv. Eng. Mater.* 8 (2006) 511–533.
- [22] S. Sarbishei, M.A. Faghihi Sani, M.R. Mohammadi, *Vacuum* 108 (2014) 12–19.
- [23] A.L. Yerokhin, A. Shatrov, V. Samsonov, P. Shashkov, A. Leyland, A. Matthews, *Surf. Coat. Technol.* 182 (2004) 78–84.
- [24] S.L. Aktuğ, S. Durdu, I. Kutbay, M. Usta, *Ceram. Int.* 42 (2016) 1246–1253.
- [25] L. Wang, J. Zhou, J. Liang, J. Chen, *Appl. Surf. Sci.* 280 (2013) 151–155.
- [26] A.L. Yerokhin, X. Nie, A. Leyland, A. Matthews, S.J. Dowey, *Surf. Coat. Technol.* 122 (1999) 73–93.
- [27] ISO 14916, *Thermal Spraying-Determination of Tensile Adhesive Strength*, 1999.
- [28] A.R. Rafieerad, M.R. Ashra, R. Mahmoodian, A.R. Bushroa, *Mater. Sci. Eng. C* 57 (2015) 397–413.
- [29] R. Arrabal, E. Matytkina, T. Hashimoto, P. Skeldon, G.E. Thompson, *Surf. Coat. Technol.* 203 (2009) 2207–2220.
- [30] E. Erfanifar, M. Aliofkhaezrai, H.F. Nabavi, H. Sharifi, A.S. Rouhaghdam, *Mater. Chem. Phys.* 185 (2017) 162–175.
- [31] V. Rezaite, L. Deresh, *Prot. Met.* 42 (2006) 368–372.
- [32] V. Raj, M.M. Ali, *J. Mater. Process. Tech.* 209 (2009) 5341–5352.
- [33] S.Y. Wang, Y.P. Xia, L. Liu, N.C. Si, *Ceram. Int.* 40 (2014) 93–99.
- [34] L. Fang, B. Zhang, W. Li, X. Li, T. Xin, Q. Zhang, *Superlattices Microstruct.* 75 (2014) 324–333.
- [35] Y. Zhao, Z. Li, Z. Lv, X. Liang, J. Min, L. Wang, Y. Shi, *Mater. Res. Bull.* 45 (2010) 1046–1050.
- [36] J. Das, S.K. Pradhan, D.R. Sahu, D.K. Mishra, S.N. Sarangi, B.B. Nayak, S. Verma, B.K. Roul, *Physica B* 405 (2010) 2492–2497.
- [37] H. Tamura, *J. Colloid Interface Sci.* 279 (2004) 1–22.
- [38] I. Yu, S. Jou, C. Chen, K. Wang, L. Pang, J.S. Liao, *Forensic Sci. Int.* 207 (2011) 14–18.
- [39] L. Wang, T. Shinohara, B.P. Zhang, *Appl. Surf. Sci.* 256 (2010) 5807–5812.
- [40] F. Jamali-Sheini, K.R. Patil, D.S. Joag, M.A. More, *Appl. Surf. Sci.* 257 (2011) 8366–8372.
- [41] Y. Rao, W. Wang, F. Tan, Y. Cai, J. Lu, X. Qiao, *Appl. Surf. Sci.* 284 (2013) 726–731.
- [42] B. Pandey, S. Ghosh, P. Srivastava, D. Kabiraj, T. Shripati, N.P. Lalla, *Physica E* 41 (2009) 1164–1168.
- [43] H.Y. Wong, C.W. Ong, R.W.M. Kwok, K.W. Wong, S.P. Wong, W.Y. Cheung, *Thin Solid Films* 376 (2000) 131–139.
- [44] R.H.U. Khan, A. Yerokhin, X. Li, H. Dong, A. Matthews, *Surf. Coat. Technol.* 205 (2010) 1679–1688.
- [45] R.O. Hussein, X. Nie, D.O. Northwood, *Electrochim. Acta* 112 (2013) 111–119.
- [46] D.E. Packham, *Int. J. Adhes. Adhes.* 23 (2003) 437–448.
- [47] Y. Yan, Y. Han, D. Li, J. Huang, Q. Lian, *Appl. Surf. Sci.* 256 (2010) 6359–6366.
- [48] E. Brodu, M. Balat-Pichelin, J.-L. Sans, J.C. Kasper, *J. Alloy. Compd.* 586 (2014) 510–517.
- [49] S. Edalatpour, M. Francoeur, *J. Quant. Spectrosc. Radiat.* 118 (2013) 75–85.
- [50] F. Ghmari, T. Ghbara, M. Laroche, R. Carminati, J.-J. Greffet, *J. Appl. Phys.* 96 (2004) 2656–2664.
- [51] Z. Yao, P. Ju, Q. Xia, J. Wang, P. Su, H. Wei, et al., *Surf. Coat. Technol.* 307 (2016) 1236–1240.
- [52] G. Wu, D. Yu, *Prog. Org. Coat.* 76 (2013) 107–112.
- [53] C.D. Wen, I. Mudawar, *Int. J. Heat. Mass. Transf.* 49 (2006) 4279–4289.
- [54] C. Li, J. Lv, Z. Liang, S. Yao, *Opt. Mater.* 35 (2013) 586–589.
- [55] J. Lv, C. Li, *Nucl. Instrum. Methods Phys. Res. Sect. B* 375 (2016) 5–7.
- [56] M.M. Mikhailov, V.A. Vlasov, S.A. Yuryev, V.V. Neshchimenko, V.V. Shcherbina, *Dyes Pigment.* 123 (2015) 72–77.
- [57] M.M.S. Al Bosta, K.J. Ma, H.H. Chien, *Infrared Phys. Technol.* 60 (2013) 323–334.
- [58] Y.M. Wang, H. Tian, X.E. Shen, L. Wen, J.H. Ouyang, Y. Zhou, et al., *Ceram. Int.* 39 (2013) 2869–2875.
- [59] D. Ma, C. Lu, Z. Fang, W. Yan, L. Wei, Y. Ni, et al., *Appl. Surf. Sci.* 389 (2016) 874–881.
- [60] S. Lu, W. Qin, X. Wu, X. Wang, G. Zhao, *Mater. Chem. Phys.* 135 (2012) 58–62.
- [61] Y.M. Wang, Y.C. Zou, H. Tian, L.X. Guo, J.H. Ouyang, D.C. Jia, et al., *Surf. Coat. Technol.* 294 (2016) 102–108.
- [62] S. Kalyanaraman, P.M. Shajinshinu, S. Vijayalakshmi, *J. Phys. Chem. Solids* 86 (2015) 108–113.
- [63] A.K. Sharma, N. Sridhara, *Adv. Space Res.* 50 (2012) 1411–1424.